Original Article

Institution of MECHANICAL ENGINEERS

Journal of AEROSPACE ENGINEERING

Proc IMechE Part G:
J Aerospace Engineering
2016, Vol. 230(12) 2179–2194
© IMechE 2015
Reprints and permissions:
sagepub.co.uk/journalsPermissions.nav
DOI: 10.1177/0954410015621928
uk.sagepub.com/jaero

SAGE

The effect of end wall boundary layer on matching and corresponding flow control technique for multistage axial compressor

Li Zhihui[1,2], Zheng Xinqian[2], Liu Yanming[1], Li Qiushi[3] and Ji Baohua[1]

Abstract

The development pattern of the end wall boundary layer (BL) in whole conditions and its effect on the matching of multistage compressor have been studied in detail in this paper. Moreover, one method of end wall zone blade modification is carried out, using computational fluid dynamics, to improve the stage matching by re-camber. It is found that the pitch-averaged thickness of end wall BL gradually increases along streamline direction and the BL is highly skewed in the pitchwise direction. In addition, the value of BL thickness, mainly depends on the stage pressure rise coefficient $\Delta p/\rho V_x^2$. For a fixed rotating speed, the axial BL displacement thickness is changed dramatically from choked condition to near surge operating point. However, this thickness shows insensitive to the change of rotating speeds. On the other hand, BL degrades the pressure-rise characteristics of stages with low efficiency, and it results in mismatching of the compressor stage. Furthermore, the deviation angle of the blades is strongly affected by the end wall BL. Finally, two rows of stators are re-cambered on the leading edge to improve the matching near the hub region where it is influenced by end wall BL. The results show that the total pressure loss coefficient of the stators is reduced by 0.6 points and 1.73 points each. Moreover, the overall isentropic efficiency of multistage compressor is enhanced by 0.39 points without compromising pressure-rise capability and surge margin.

Keywords

Boundary layer, end wall, multistage axial compressor, stage matching, flow control

Date received: 17 February 2015; accepted: 9 November 2015

Introduction

It is well known that the aerodynamic performance of multistage axial compressors such as pressure rise, stall point, and efficiency are strongly limited by boundary layer (BL) development. In addition, it introduces considerable three dimensionality and unsteadiness in flow. For example, Wisler[1] suggested that more than half of losses in an axial compressor is associated with the flow in the end wall region. However, study of BL behavior inside a compressor is complicated and difficult to examine experimentally. Thus far, this question stands as the most critical aspect of a multistage compressor for designers.

Previous attempts to analyze the flow were based on this simplification that the flow is circumferentially or passage averaged, to be compatible with the commonly available axisymmetric models of the mainstream flow. This method neglected the complex interactions in the end wall regions. During this period, Mellor and Wood[2] stated an end wall BL theory which introduced the concepts such as axial, tangential defect force thickness, etc. Furthermore, Hirsch[3] modified a theory formulated originally by Mellor by incorporation of the shape factor variation and the effects of Reynolds number as well as introduction of the wall skewing angle. In addition, Ruyck and Hirsh[4] introduced an axial compressor end wall BL theory which is required the introduction of three-dimensional (3D) velocity profile models and allowed a prediction of radial distribution of velocities and flow angles including the end wall region.

As for the experimental respect, a large number of studies have been undertaken, some specifically to provide data for checking theoretical models, others

[1]School of Aerospace Engineering, Beijing Institute of Technology, Beijing, China
[2]State Key Laboratory of Automotive Safety and Energy, Tsinghua University, Beijing, China
[3]National Key Laboratory on Aero-engines, School of Energy and Power Engineering, Beihang University, Beijing, China

Corresponding author:
Liu Yanming, School of Aerospace Engineering, Beijing Institute of Technology, Beijing, China.
Email: liuym@bit.edu.cn

to gain some insight into the physical nature of flow processes. For example, Smith[5] claimed a repeating-stage flow model and experimental data. He finally found that end wall BL thickness primarily depends on the blade-to-blade passage width, the aerodynamic loading level and clearances. Moreover, Hunter and Cumpsty[6] did an investigation experimentally on an isolated rotor and they found that the tip clearance had pronounced effects upon BL development and the downstream BL thicken as the rotor loading and the blade-end clearance size were increased. Similarly, Lakshminarayana[7,8] made detailed measurements about BL development on casing wall and the complex interactions between the leakage flow and the annulus BL. However, measurements inside compressor are complicated, especially on the rotors, since the measuring probes have to be employed in a narrow space or rotate with the rotors. There is not complete data available for these regions.

Much more research effort has been concerned with the development of BL itself; on the other hand the matching problem caused by end wall region flow is a cursing problem for the compressor designers. Basically, at the design point, the choices of the airfoil and the flow path cross-sectional area for each stage depend on a correct prediction of upstream stage performance. Any slight discrepancy on the upstream stages prediction will modify the performance of downstream stages, hence further affecting the overall performance. More difficulties follow with the fact that the downstream stages performance will in turn modify the performance of upstream stages. This issue was raised by Stone[9] in the early years of multi-stage axial flow compressor design. Kua[10] described the general rules of matching multistage compressor and discussed about the design of the tip clearance. Domercq and Escuret[11] underlined how the tip clearance flow affects the matching of compressor stages, hence modifying the efficiency and stall margin of the compressor. Their conclusion was that the magnitude of the pressure ratio due to the open tip clearance and the induced mismatching has to be taken into account in order to obtain a robust design. Furthermore, the evolution of the flow angle is one of the key parameters in the stage matching. Indeed, Carter's Rule[12] provided a 2D flow deviation angle model. Then he modified the forms of Carter's Rule to account for the effects of radius and axial velocity changes which were experimentally measured. These simpler correlations gave a fast access to matching prediction. However, when blading was applied in the true axial compressors environment, the interaction with the end wall causes a divergence from 2D predictions and it was necessary to take the effect of end wall BL development into account. Roberts[13] introduced a semi-empirical deviation angle model that allowed reasonable estimates of various 3D viscous effects for subsonic, axial compressor middle stages and it predicted the variation of spanwise deviation to a good approximation. However, these models which are mentioned above contained lots of empirical parameters and assumptions and they could not achieve satisfactory accuracy on the effect of end wall stage matching.

In order to improve the performance of compressor, flow control measures are necessary, especially near the end wall region. Thus far, many kinds of flow control researches[14–21] have been done to improve the compressor performance. Re-cambered design (also called end-bend) is one of the effective methods to achieve improvement in the end wall region. Wisler[1] and Freeman[22] applied it in engine compressor and recognized its effectiveness on reducing the losses. Gallimore et al.[23,24] treated "end-bend" as a 3D blade design method and applied it successfully on high-pressure compressors. George et al.[25] applied the end-bend on stators and they found that the hub loading of the blade was improved with the smaller secondary flow. Luo et al.[26] conducted an experimental investigation on the 2-stage compressor with bowed cantilevered stators and the leakage vortex, corner stall and passage cross flow were eliminated obviously.

The objective of this paper is to summarize the pattern of BL development in the full operating regions of a typical well-designed 5-stage compressor and explore its flow mechanism. Then the major effect of end wall BL on stage matching is discussed. Finally, one type of flow control technique, by which re-camber on the leading edge (LE) is applied near hub end wall region, is imposed on two stator rows to improve the stage matching and the corresponding quantitative angle modification is based on deviation angle results derived from computational fluid dynamics.

Computational methods

The design parameters of the multistage compressor rig are summarized in Table 1, where the hub/tip radius ratio and solidity values are derived from R1 row. A single passage computational domain, including IGV, rotors and stators, is shown in Figure 1. ANSYS/CFX software package is employed to simulate the flow in different conditions.

Grid generation

Grid topology selected for flow analysis and modification is generated by ANSYS/Turbogrid. Multiblock structured grids with hexahedral elements are used in this study. Around blade surfaces the O-grid with adequate number of elements are employed for a better BL resolution. The grid node number inside BL is larger than 10. The J-grid topology is used on the leading edge and trailing edge of the blade, whereas H-grid meshes are used at the inlet, passage and outlet. In order to simulate the viscous flow accurately, the distance between the first cell and solid wall is set to 1e−6 m. After the simulation, the

Table 1. The design parameters of the multistage rig.

Parameter	Value
Flow coefficient	0.53
Inlet tip Mach number	1.45
Specific speed	4.88
Hub/tip radius ratio	0.50
Solidity	1.54

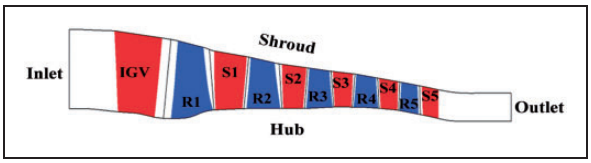

Figure 1. The single computational passage domain.

maximum y^+ near the trailing edge of the blade is found to be between 4 and 5 while the value of the y^+ near the hub surface is less than 2. It should be noticed that wall functions are not used here. The grid dependence has been finished and the total grid number is almost 3.3 millions (shown in Figure 2).

Numerical method

Flow solver CFX/ANSYS software package is adopted to simulate the viscous flow of high-turning compressor. Second-order difference scheme is employed to discrete the Reynolds-averaged N-S equation in space and achieve convergence solution. A value of 5e−5 has been chosen as the maximum residual for convergence criterion.

Boundary conditions

Total pressure and total temperature are imposed averagely at the inlet, whereas average static pressure and total temperature are specified at the outlet. By increasing static pressure at the outlet plane, the performance of the compressor is obtained, and the last stable operating point is considered as the steady near-stall point for the compressor. A "frozen rotor" interface is chosen between domains. The shear stress transport (SST) turbulence model is used because of its known effectiveness in treating flows with adverse pressure gradients and separating flow. Turbulence intensity of 5% (medium intensity) is chosen. It should be emphasized that the variable geometry technique is applied in front stator rows (IGV, S1, and S2) of the multistage compressor.

Numerical method validation

The numerical method mentioned above is validated by the application on Rotor 37. In the front stages of the multistage compressor, the transonic field

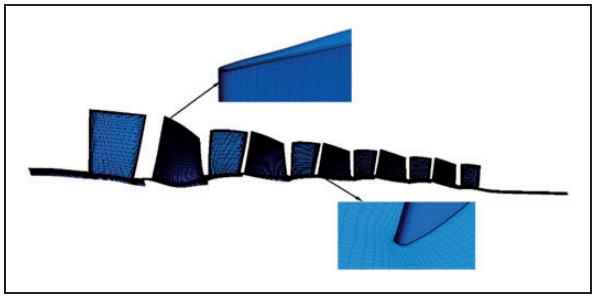

Figure 2. The grid generation scheme.

occurred, which is similar to the Rotor 37. In addition, the grid topology, distributions and total number of the Rotor 37 case are almost the same with the front stages, i.e. the O-grid near wall, the J-grid on the leading/trailing edge and the H-grid at the inlet are used here. The detail grid generation scheme of Rotor 37 is shown in Figure 3. The numerical result is compared with experimental data shown in the open literature, which is shown in Figure 4. It is shown that the numerical result has a satisfying agreement with experimental data. Hence, the reliability of the method used here has been validated.

The normalized pressure ratio and isentropic efficiency with the normalized mass flow rate of the 5-stage compressor is shown in Figure 5. Three rotating speeds which are the cruising speed (100%), accelerating speed (105%), and decelerating speed (95%) are simulated respectively.

Boundary layer development pattern

With the BL theory of end wall flow treated as a viscous flow problem, the thickness development of the flow near the end wall region is concerned and described by the overall defect integral properties rather than in terms of detailed BL profiles themselves. Before studying the BL development, the identification of wall BL edge should be made. Just as Hunter and Cumspty described as follows, the most convenient definition appeared to be the position where the axial velocity either reached a peak or reached the uniform value of the free stream.

Velocity profiles of hub end wall BL

In this paper, we mainly focus on the axial end wall BL development of multistage compressor. As the definition of BL was mentioned above, the axial velocity profiles on the peak efficiency operating point of cruising speed, which is circumferentially mass-averaged downstream each rotor and stator, are shown in Figure 6.

Red points in Figure 6 represent the places where axial velocity magnitude reaches the maximum for the first time in the spanwise direction. Therefore, it means that the edge of end wall BL by the definition mentioned above. There is a pronounced broadening

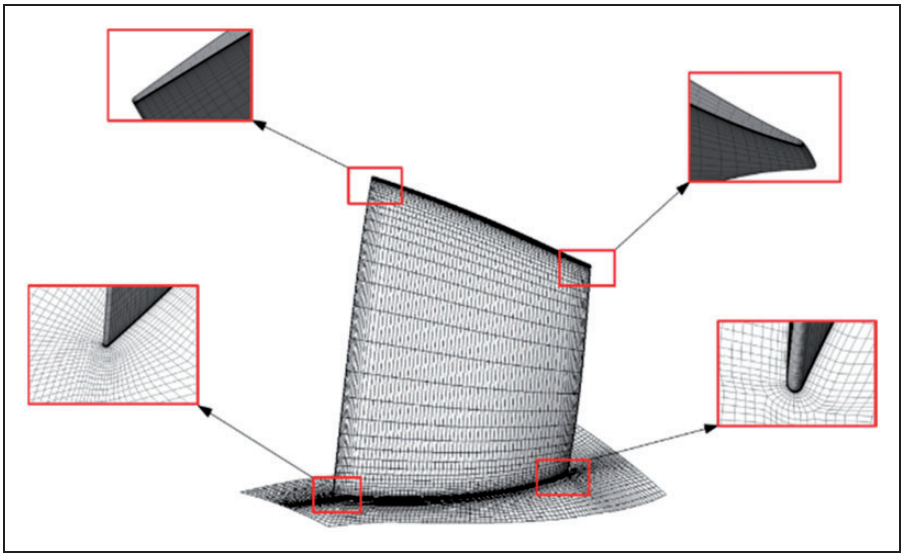

Figure 3. The grid generation scheme of Rotor 37.

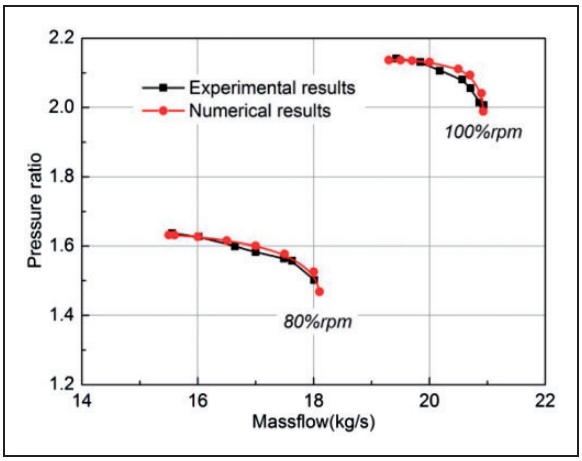

Figure 4. Numerical method validation on Rotor 37.

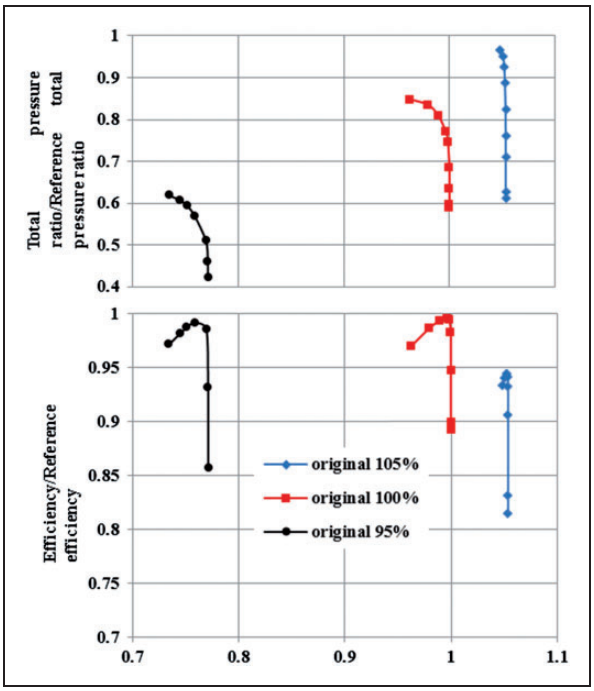

Figure 5. Overall performance characteristics of multistage compressor.

of the region of the BL across the rotor and stator along the axial direction, and the profiles become less full with increasing stage number. Obviously the development of BL thickness should be normalized for convenient comparison, and the quantitative development would be described by the integral parameter of axial velocity.

Integral development pattern of end wall BL

The concept of BL displacement thickness is illustrated in Figure 7. The challenges associated with defining BL region in a compressor blade row flow field are that the flow is multidirectional, and the free stream is nonuniform. The integral parameter displacement thickness δ^*, which is convenient to compare, is introduced here

$$\delta^* = \int_0^{\delta} \left(1 - \frac{\rho v_x}{\rho_V V_x}\right) \mathrm{d}z \tag{1}$$

where ρ is the air density and the integral is taken along the blade direction z. Here, v stands for flow velocity inside BL while V_x and ρ_V are the maximum value of $v_x v$ and ρ at the BL edge.

A simple analysis of BL along the end wall is given in Figure 8, in which the geometry for the case of a blade with clearance is shown. The view shows an axial section through the machine.

Here, V_{x1} and V_{x2} indicate the mainstream velocity on A and D at two different streamwise locations. The BL edge height [δ_1 and δ_2] are resulted from the definition mentioned above. We assume that$F_x$is the axial component of blade force at the edge of BL

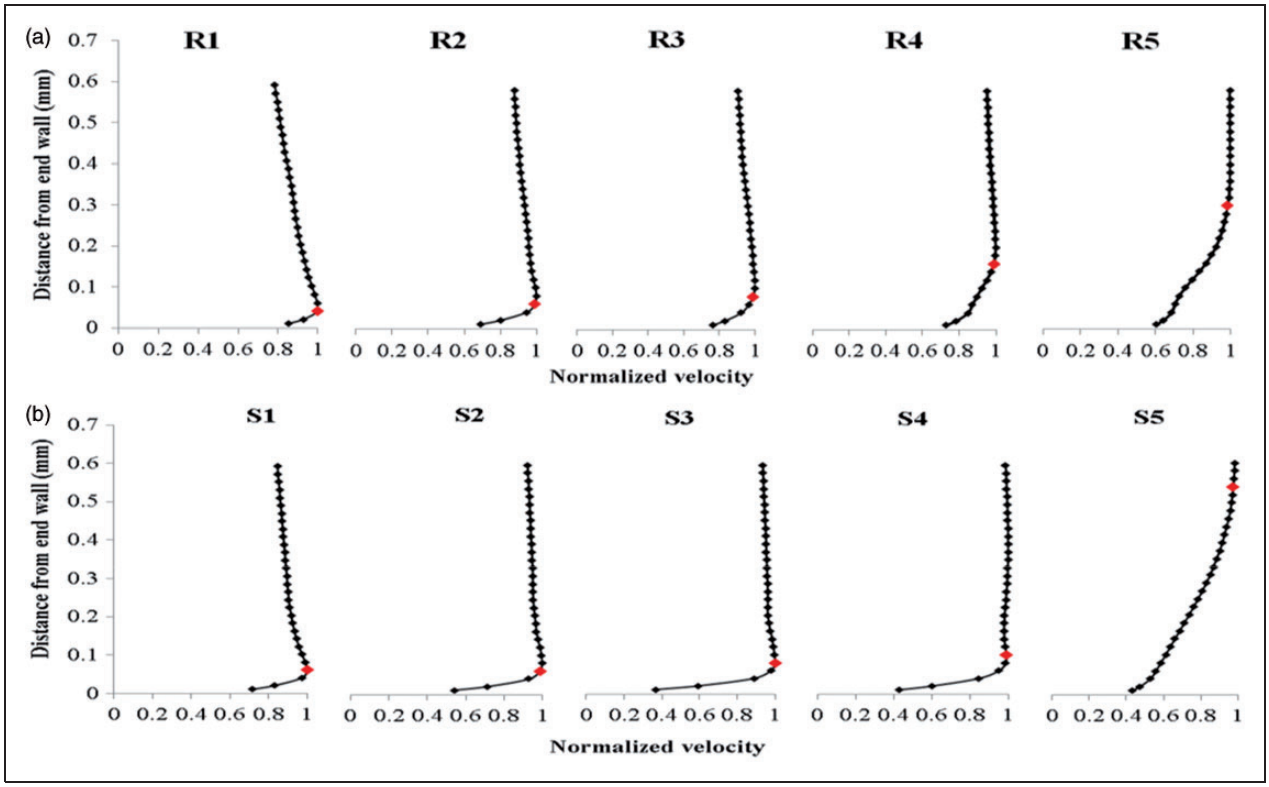

Figure 6. Velocity profiles downstream of (a) rotors and (b) stators.

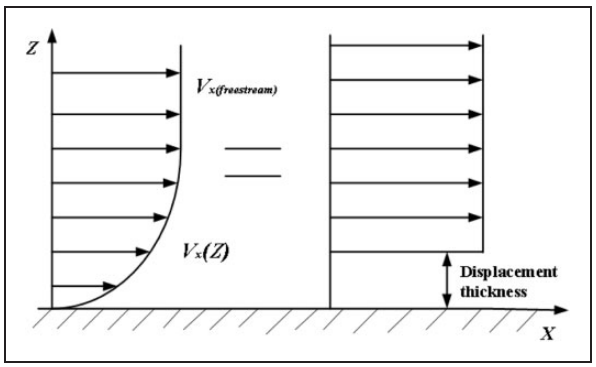

Figure 7. BL schematic.

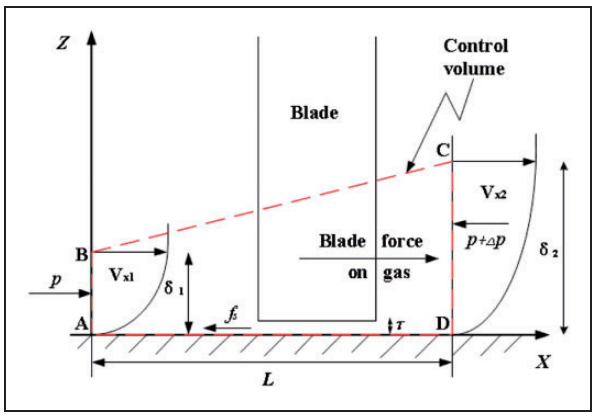

Figure 8. Analysis of BL development.

andδ_{Fx}denotes the deficit thickness of the axial force. Furthermoreτdenotes the height of hub clearance and$f_s$is the end wall shear stress in the axial direction.

In the case of conservation of axial momentum in the control volume, the equation of momentum is

$$\int_0^{\delta 1} s\rho v_{x1}^2 dz - \int_0^{\delta_2} s\rho v_{x2}^2 dz - \left(\frac{V_{x1}+V_{x2}}{2}\right) \left(\int_0^{\delta_1} \rho s v_{x1} dz - \int_0^{\delta_2} \rho s v_{x2} dz\right) = f_x sL + F_x \delta_{Fx} \quad (2)$$

where it is integrated across the pitch (s) at each radius. The integral is taken along the blade direction z, into the mainstream where $v_x = V_x$. Furthermore, the velocity through BC is assumed to be the average value of V_{x1} and V_{x2}. L is the distance between two different stream locations.

For the convenience of comparison, the axial momentum thickness [θ_x] and the displacement thickness [δ^*] are introduced to transform the formulas, and we consider the mainstream axial velocity maintained constant, so equation (2) yielded

$$\Delta\theta = \theta_2 - \theta_1 = \frac{1}{V_x^2}\left(\frac{f_s L}{\rho} + \frac{F_x \delta_{Fx}}{\rho s}\right) \quad (3)$$

Here, the assumption of invariant pressure with radius is accepted. As a result, F_x equals to $s\Delta p$

outside the BL region, where Δp is the pressure rise across the blade. Furthermore, as mentioned by Cumpsty, the skin friction coefficient is normally of order 0.003 for turbulent BL at fairly high Reynolds numbers. Thus the component of the wall shear stress in the axial direction is given by

$$f_s \approx 0.003(\rho V_x^2/2) \tag{4}$$

Empiricism in the form of a relation for the momentum thickness and displacement thickness is given by

$$H = \delta^*/\theta \tag{5}$$

Furthermore, Horlock and Perkins took δ_{Fx} to be the product of an empirical constant K and clearance size τ, implying that the local blade lift is retained to the end of a cantilevered unshrouded blade. Lakshminarayana and Horck showed progressive shedding toward the tip together with some lift retention there, suggesting that the force deficit thickness should be somewhat greater than $\tau(1 < K < 2$, say). The thickness displacement modification is then

$$\Delta\delta_x = \frac{\Delta pK\tau H}{\rho V_x^2} + 0.0015LH \tag{6}$$

It can be noted from equation (6) that, for a fixed compressor configuration, the change across the stator hub clearance row $\Delta\delta_x$ is mainly proportional to the pressure rise coefficient $\Delta p/\rho V_x^2$ (in this paper, the slash '/' means the division operation). The displacement thickness of BL increases across the cantilever stator hub clearance region. Conversely, for the rotor hub row, the blade force direction is identical to the mainstream. Therefore, the displacement thickness of BL decreases across the rotor hub row.

The variation of axial displacement thickness of BL with the change of operating point and the rotating speed is summarized in Figure 9(a). Obviously, the pattern of axial BL changes dramatically when the operating point moved from choked condition to near surge operating point. The average BL thickness growth rate near surge point is about 4 times of that at choked operating point. This phenomenon can be explained by the reason that the reverse pressure gradient and mainstream velocity values largely changes from choke to surge. Equation (6) indicates that the pressure rise coefficient term $\Delta p/\rho V_x^2$ is the most important parameters for controlling the development of BL. Thus, the BL grew rapidly when the reverse pressure gradient is higher and velocity is smaller (i.e. near surge condition). Oppositely, the BL thickness evolves slowly when the reverse pressure gradient is gentle with big mainstream magnitude (i.e. near choked condition). Furthermore, the pattern of BL is nearly insensitive to the change of rotating speed. The BL development near surge operating point with three different rotating speeds seemed to be similar, so did the peak efficiency and near choked operating points. This phenomenon also could be explained by the effect of the pressure rise coefficient term. For example, when the operating point moves from high rotating speed to low rotating speed, both the reverse pressure gradient and the main flow velocity decrease. As a result, the growth of BL displacement thickness maintained the same order as the former condition.

Although the displacement thickness of stage hub end wall BL increases in the mainstream direction, Figure 9(b) shows that the thickness increases when the stream flow through the cantilevered stator row and decreases through the rotor row of one stage. All of the data derived from either the edge of BL or the displacement thickness dedicate that the end wall BL results in more serious influence along the streamwise direction.

Losses distribution near end wall region

The thickness of BL as discussed before has influence on the performance of compressor (i.e. the loss distribution) and it should be emphasized. Here, the total pressure loss coefficient η_T is used for the stator and isentropic efficiency η_{Isen} for rotor to evaluate the effect of end wall BL on the performance of compressor.

The definition of pressure loss coefficient and isentropic efficiency are introduced here

$$\eta_T = \frac{P_T^{in} - P_T^{out}}{P_T^{in} - P_S^{in}} \tag{7}$$

$$\eta_{Isen} = \frac{(P_T^{out}/P_T^{in})^{(\gamma-1)/\gamma} - 1}{(T_T^{out}/T_T^{in}) - 1} \tag{8}$$

where γ is ratio of specific heats, P_T, P_S, and T_T are total pressure, static pressure, and total temperature, respectively. Losses distribution at the operating point (OP), which is circumferentially mass averaged, is shown in Figure 10.

The loss is big in the end wall region and the value increased along the streamwise direction, which is similar with the displacement thickness pattern in some extent. Moreover, the scope of losses is broadened in the spanwise direction. It is reasonable that the corner stall flow, passage cross vortex and clearance leakage produced lots of hub losses in rear stages. End wall losses play a significant role in the total losses of the compressor.

Furthermore, to observe the tangential and radial situation, the relative exit Mach number contours in the third stage passage, which is representative to the five stage pitchwise flow, are shown in Figure 11.

In Figure 11, the dashed line indicates the edge of end wall BL. The skew of BL close to the end wall could be observed clearly. The stall corner vortex near

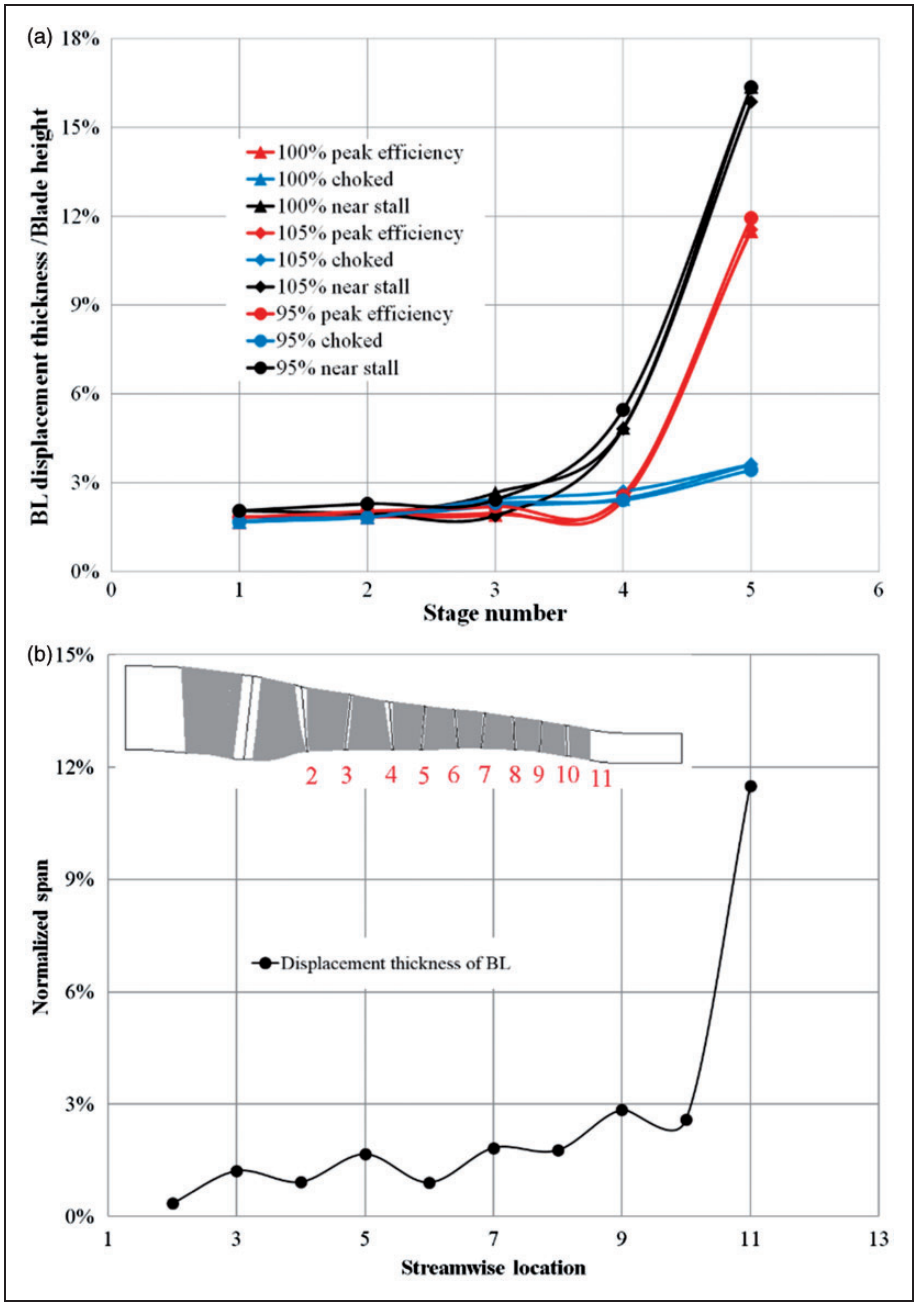

Figure 9. Variation of displacement thickness of BL: (a) normalized BL displacement thickness versus variable operating points; (b) normalized BL displacement thickness versus variable streamwise locations.

the suction surface (SS) and passage cross flow, which migrates from pressure surface (PS) to SS, made the BL near hub wall nonuniform in the pitchwise direction, especially for the rotor. However, the cantilevered stator suffered less influence due to the existence of hub clearance leakage flow (LF).

Effect of BL on stage matching

The basic effect of end wall BL on a single blade row consists of an increase in loss due to the interaction of end wall BL with the main flow. The purpose of this paragraph is to point out the effect of this major technological effect on stage matching.

Figure 12 gives the contours of the circumferentially averaged static entropy obtained from 3D Navier–Stokes computations of the compressor block for two levels of end wall flow, i.e. original and nominal end wall. The nominal hub end wall is done by setting the hub free slip wall boundary condition.

The difference in entropy contours emphasizes the increase in hub pressure losses and blockage located near the hub for the original configuration. Finally, the stage pressure-rise characteristics are deteriorated, resulting in a mismatching between stages. In a multistage compressor, the appearance of end wall BL of a given stage has several effects.

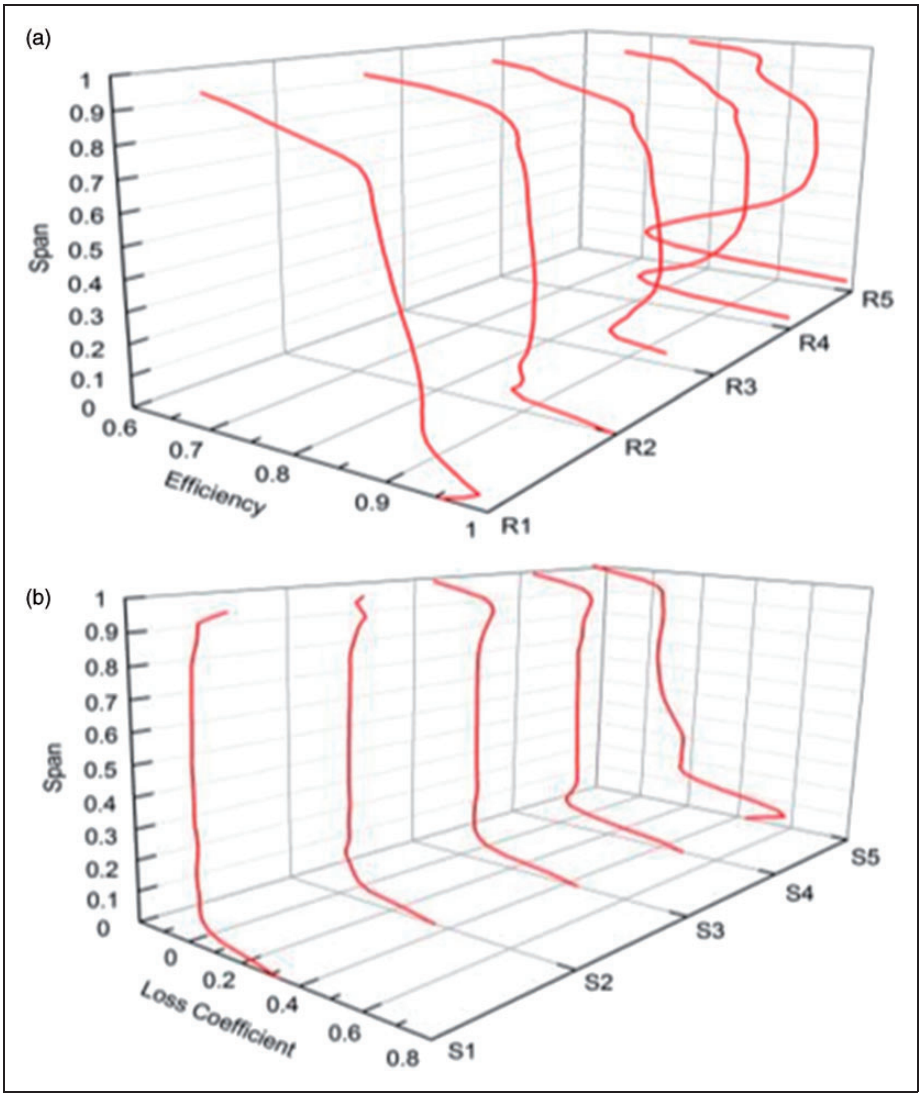

Figure 10. Losses distribution along blade height: (a) rotor isentropic efficiencyη_{Isen}; (b) stator total pressure loss coefficient η_T.

1. The pressure-rise characteristics of this stage will be degraded, with lower pressure rise capability, stall margin, and efficiency.
2. Upstream stages will be throttled to compensate for the pressure loss of the end wall flow stage.
3. Downstream stages will have to operate with an increased inlet blockage factor. This last effect will tend to move the blockage factor evolution across the compressor away from the design intent.
4. The second and third effects will result in a mismatching of compressor stages.

(a) Overall effect on stage matching of compressor

In Figure 13, we assume that one compressor contains two stages. Furthermore, the inlet mass flow rate is m, with total temperature T_1 and total pressure P_1. And the corrected mass flow for Stage 1 and Stage 2 are m_1^* and m_2^*, respectively. The difference in throttling can be calculated by expressing the ratio of the outlet to inlet corrected flow rates of a stage as a function of the pressure ratio π and the corresponding polytropic efficiencyη_{Pol}. Thus, for a perfect gas we have

$$\frac{m_2^*}{m_1^*} = \pi^{(\gamma-1-2\gamma\eta_{Pol})/2\gamma\eta_{Pol}} \tag{9}$$

Due to $\pi > 1$ and $\gamma = 1.4$, it is easy to know that the corrected mass flow rate ratio$m_2^*/m_1^* < 1$. As a result, the main effect is that the second stage is further throttled than the first stage, each stage pressure-rise characteristics is deteriorated by the end wall blockage. The corrected mass flow rate of the free slide end wall and polytropic efficiency corresponding to Stage 1 are written as m_{1n}^* and η_{nPol}. The change of corrected mass flow due to blockage is $\Delta m^* = m_n^* - m^*$. It now yields that

$$\begin{aligned}\Delta m_2^* &= m_{1n}^* \pi_n^{*(\gamma-1-2\gamma\eta_{nPol})/2\gamma\eta_{nPol}} - m_1^* \pi^{(\gamma-1-2\gamma\eta_{Pol})/2\gamma\eta_{Pol}} \\ &< (m_{1n}^* - m_1^*)\pi^{(\gamma-1-2\gamma\eta_{Pol})/2\gamma\eta_{Pol}} < \Delta m_1^*\end{aligned} \tag{10}$$

Equation (19) illustrates the point that the difference in the corrected mass flow rate is intensified by the

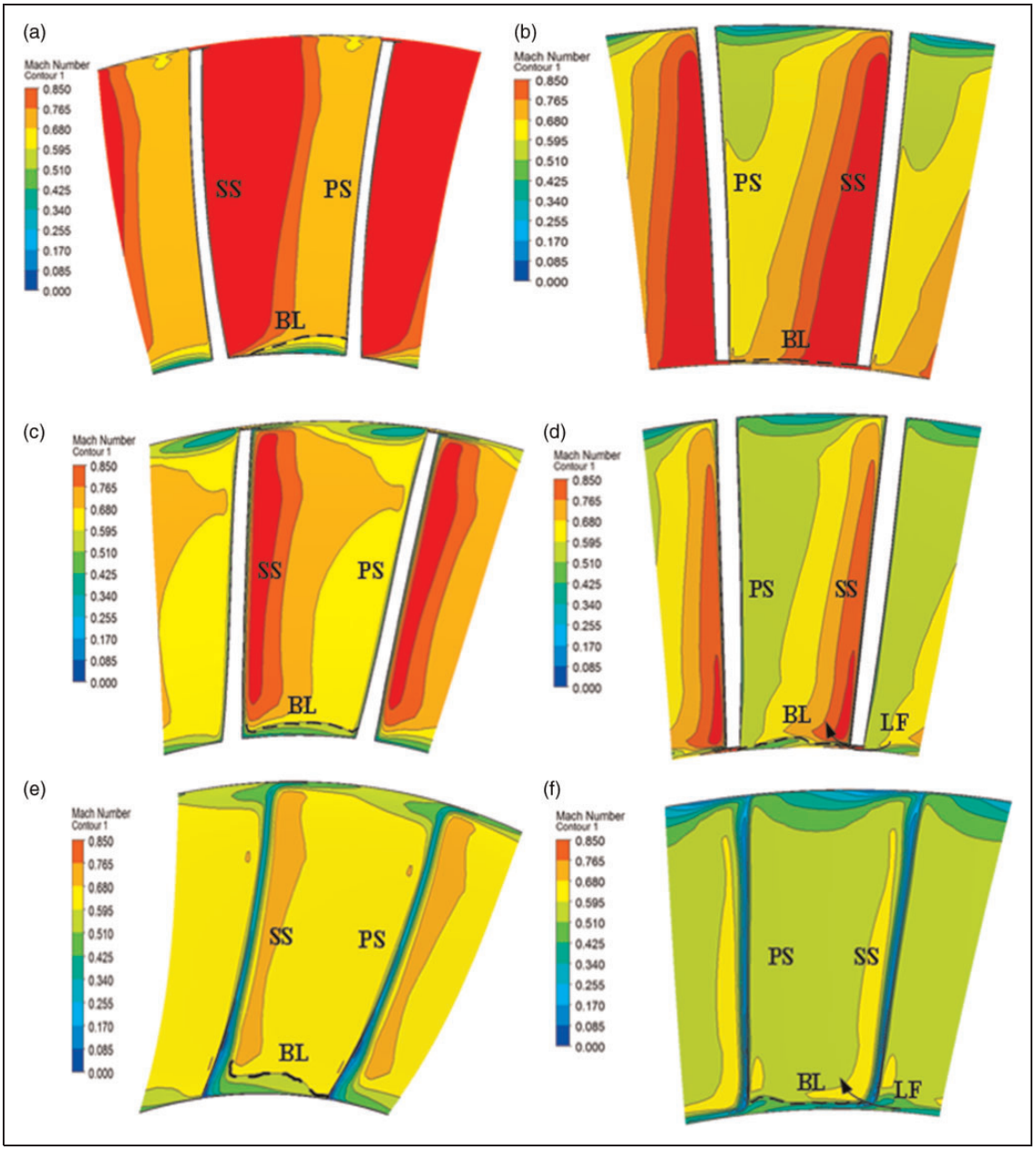

Figure 11. Contours of rotors and stators exit Mach number: (a) 20%c of R3; (b) 20%c of S3; (c) 60%c of R3; (d) 60%c of S3; (e) 90%c of R3; (f) 90%c of S3.

deterioration of each stage pressure-rise characteristics. Finally, the front stage exhibits a poor throttling capacity and the margin of all stages is limited by it. In order to prove the technical point mentioned above, the matching of detail compressor cases is shown below.

The related block aerodynamic pressure-rise characteristics are given in Figure 14. Figures (a) to (c) give the details of the individual stage behavior. In Figure (c), the existence of end wall BL results in a 1.7% pressure drop with the expected effect (0.7% decrease in stage corrected mass flow rate). Therefore, as discussed above, the outlet corrected mass flow of the fourth stage will differ from the slip and free slip case. This is the reason why the OP of the fourth stage shows a further throttling for the free slip wall case (Figure (b)). The pressure drop in the fourth stage is close to 0.8% and corresponding 1.2% difference in outlet corrected mass flow due to the end wall BL. Finally, the throttling of the third stage is increased by an amount of 2.6%.

(b) Overall effect on flow angle of compressor

To get the detailed flow information about the stage matching, the flow angle near the trailing edge of the two cases (free slip wall and no free slip wall) is compared in Figure 15.

Figure 15 indicates that the end wall BL near hub region mainly influences about 40% span of the

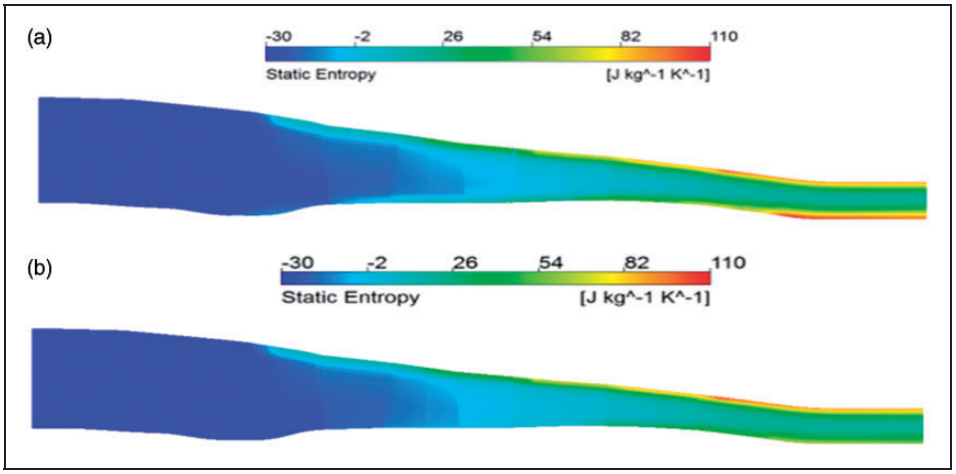

Figure 12. Contours of the circumferentially averaged static entropy: (a) Original hub end wall; (b) free slip hub end wall.

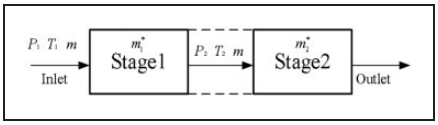

Figure 13. Scheme of corrected mass flowrate between stages.

blades both for rotor and stator. As for the rotor, the main flow is overturned close to the end wall and under-turned further away. The detail streamlines are shown in Figure 16, in which there is a corner stall near the hub region of the rotor and the trailing edge turbo surface streamlines act like a ''clockwise circle''. Likewise the flow situation on the stator blade exhibits a similar behavior, where the under-turned and over-turned flow is observed. Some difference is observed near the hub wall of the stators. Because of the tip clearance of cantilever stator, the clearance flow makes the flow swirl far from the prototype.

Flow control method

Deviation angle correlation

As shown above, the BL thickness increases aggressively along axial direction and seriously affects the efficiency especially in rear stages. Corner stall and leakage flow make the matching between stages very terrible in the end wall region. For a designer, it is difficult to evaluate the effect in the design progress from the traditional method mentioned above. However, the 3D flow field calculation provides tool for us to achieve quantitative flow details and make effective optimizations according to the accurate result. In this paper, we focus on the rear stages of axial compressor for the reason that the end wall BL developed fully in this area. In order to validate the modification method and simplify the progress, the corresponding flow angle and blade angle derived from leading edge of S4 and S5 are shown in Figure 17.

Because of the deviation angle of the rotor near the hub and shroud is big, the mismatching (mainly the incident angle) with downstream stators would be substantial. Figure 16 indicates that the deviation angle of R4 and R5 are individually overturned by almost 8° and 11° near hub end wall. In order to eliminate the mismatching caused by end wall BL, the quantitative re-camber technique (also called ''end bend'') is applied in the next procedure.

Leading edge re-camber

In a typical multistage compressor, the viscous forces exerted on the flow near the end wall, change in the frame of reference between rotors and stators and the secondary flows produced by upstream blade rows, cause the flow angle at the inlet to the blade rows typically to increase (measured from the axial direction) progressively as the end wall is approached. As we known, aligning the leading edge to the flow direction could make the suction surface deceleration smaller and prevent the BL from separating. The leading edge re-camber method is developed by this means.

In this paper, hub incident angle is modified on S4 and S5. For S4, the leading edge blade angle up to 20% span measured from the axial direction is turned to match the flow angle, which is based on the flow angle shown in Figure 16. Then the new downstream flow situation (S5) is calculated. Although this new inlet flow angle for S5 is not plot here, the leading edge blade angle is turned to match the flow angle based on the calculation result (also up to 20% span). Moreover, the centroid stacking is kept same with the original geometry. The back version view comparison between original and modified blade is shown in Figure 18.

A comparison between original and modified total compressor performance characteristics are shown in

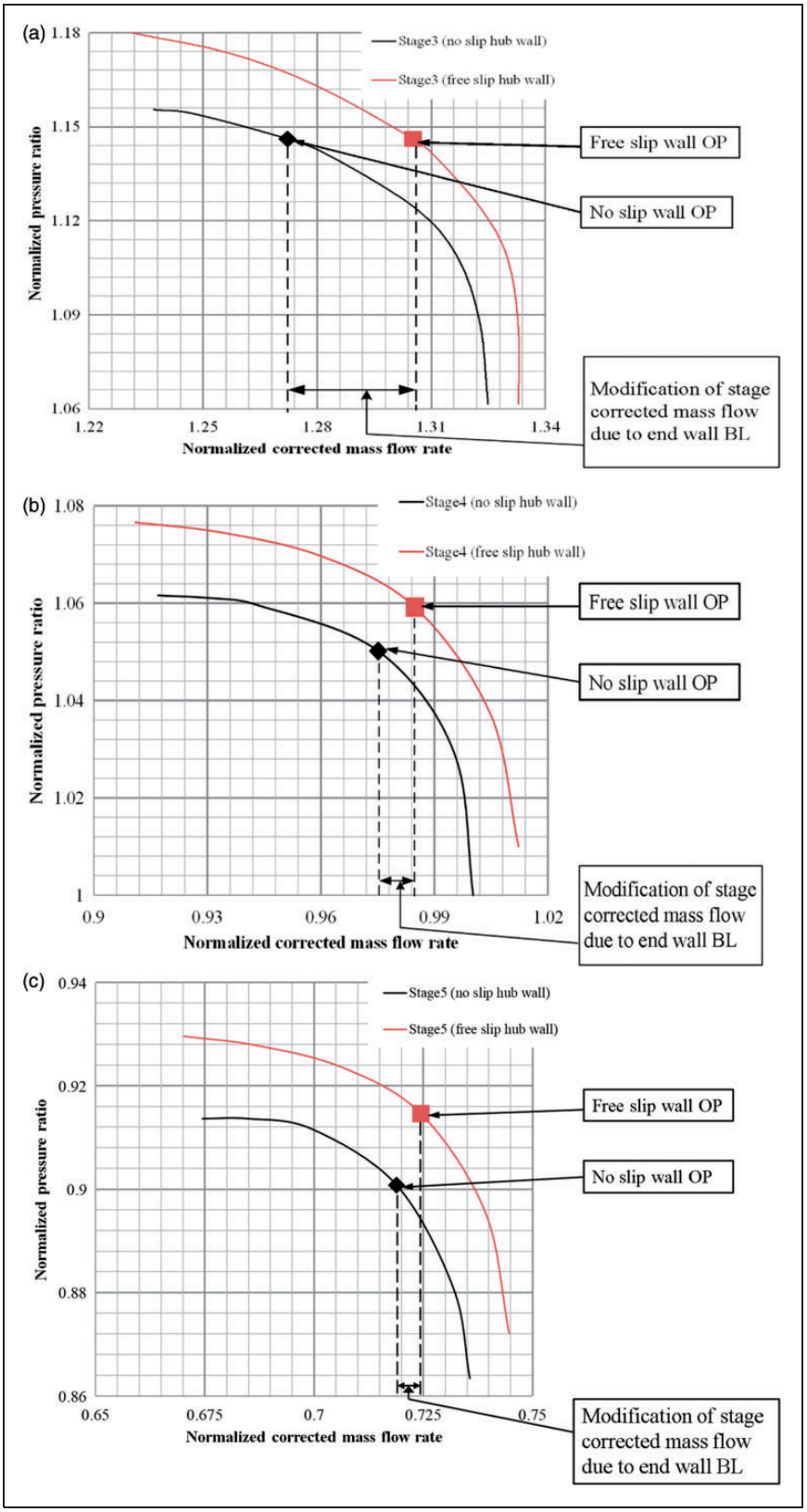

Figure 14. Matching of the rear block of stages: (a) third stage compressor map; (b) fourth stage compressor map; (c) fifth stage compressor map.

Figure 19. The peak isentropic efficiency is increased by 0.39 points while the stable region and the total pressure rise remain same with the origin. It is also found that the total pressure losses coefficient of S4 is reduced by 0.6 points and 1.73 points to S5, which is shown in Figure 20.

Figure 20 indicates that the end wall and the middle span region loss reduction are improving.

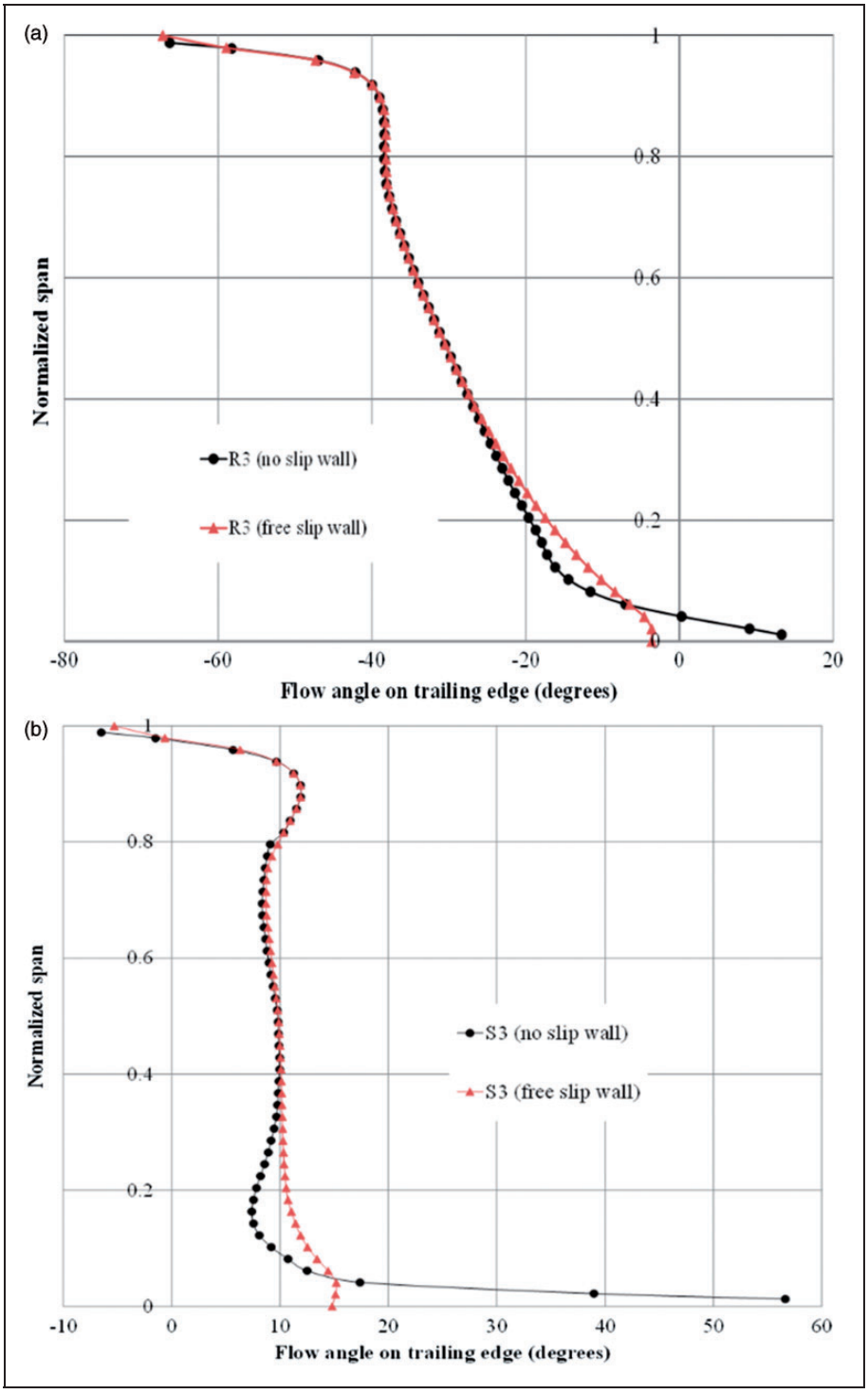

Figure 15. Comparison of flow angle on trailing edges: (a) R3 flow angle on trailing edge; (b) S3 flow angle on trailing edge.

The end wall loss is relieved due to the effect of re-camber. Moreover, this middle span region change might be caused by the introduction of sweep and dihedral more or less, which is the result of modifying the stacking line besides the centroid line. Furthermore, both of the performance of fourth and fifth stage have been improved. All of these improvements show that the design intent of improving the datum compressor behavior has been maintained.

Over all, the flow mechanism of performance improvement can be divided into two parts:

1. Aligning the leading edge more to the flow direction can help to reduce the amount of deceleration near suction surface, reduce the pressure rise and finally suppress the BL separation.
2. Stacking line choices incorporating re-camber introduce effects of dihedral and sweep (especially dihedral effect near hub shown in Figure 18). As to

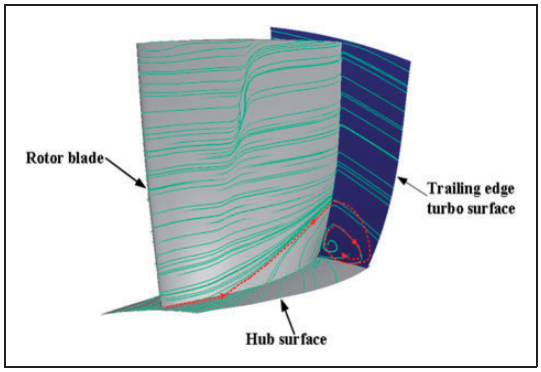

Figure 16. Surface streamlines of rotor.

the dihedral effect defined by Gallimore et al.,[23,24] the stacking line mainly introduces positive dihedral in this paper. Changes of blade loading caused by the induced velocity field in this region have a significant effect on end wall loss generation. Positive dihedral can reduce the blade force local to the end wall and alleviate suction surface deceleration, leading to a fuller velocity profile near the end wall.

As a result, the loss can be reduced near the end wall, resulting in the total performance improvement.

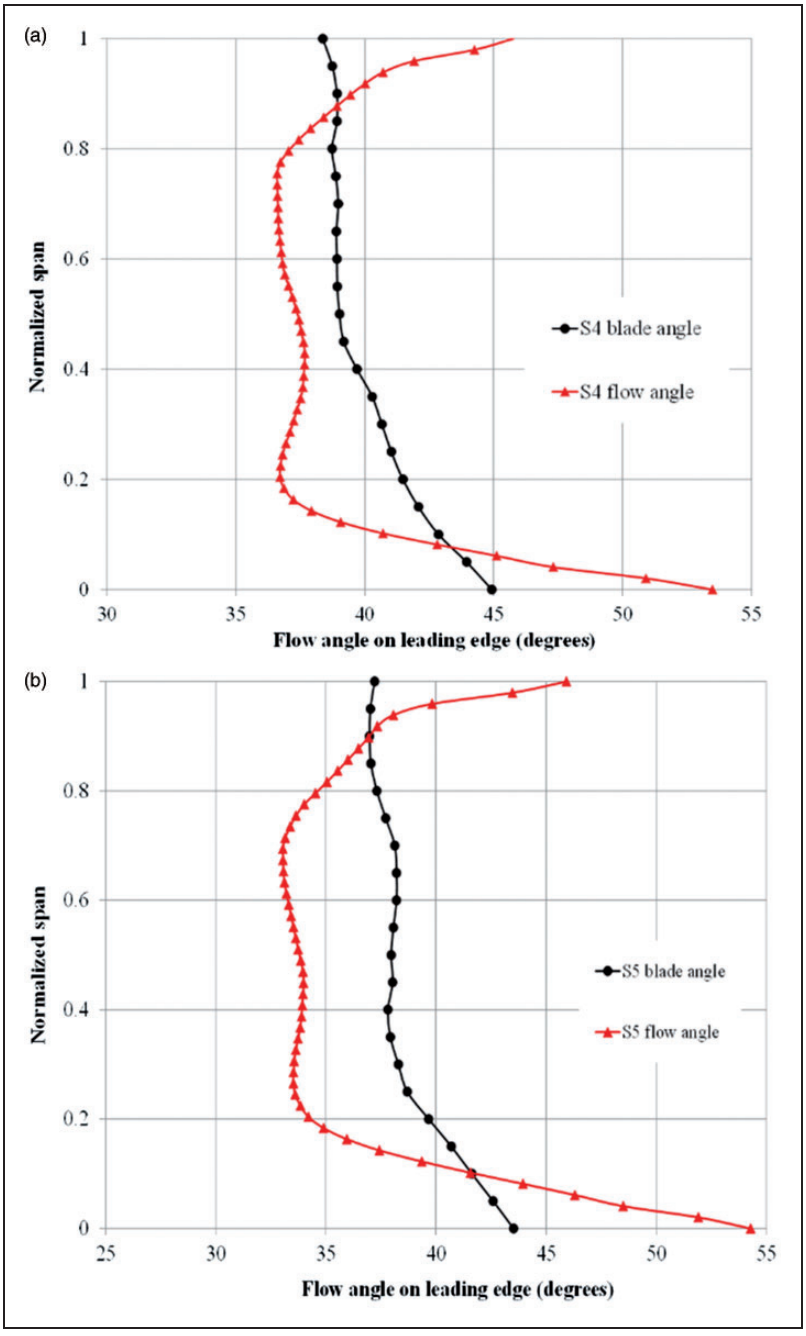

Figure 17. Deviation correlation of: (a) R4 and (b) R5.

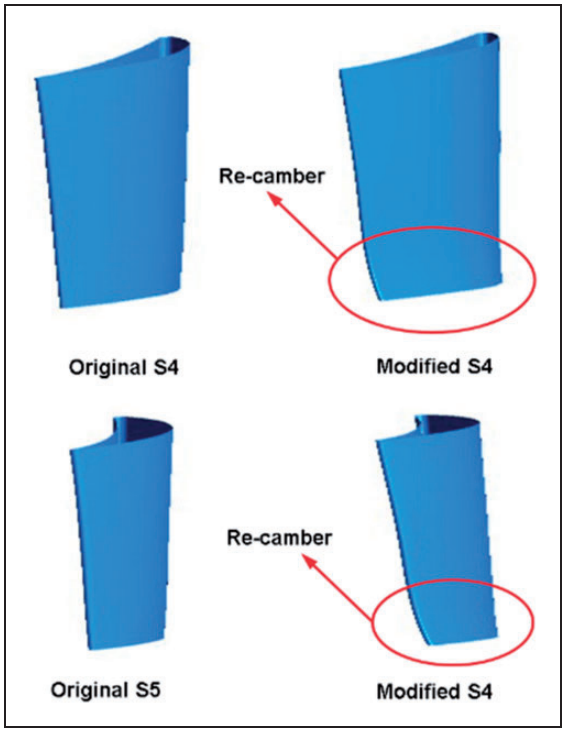

Figure 18. Comparison between origin and modified geometry.

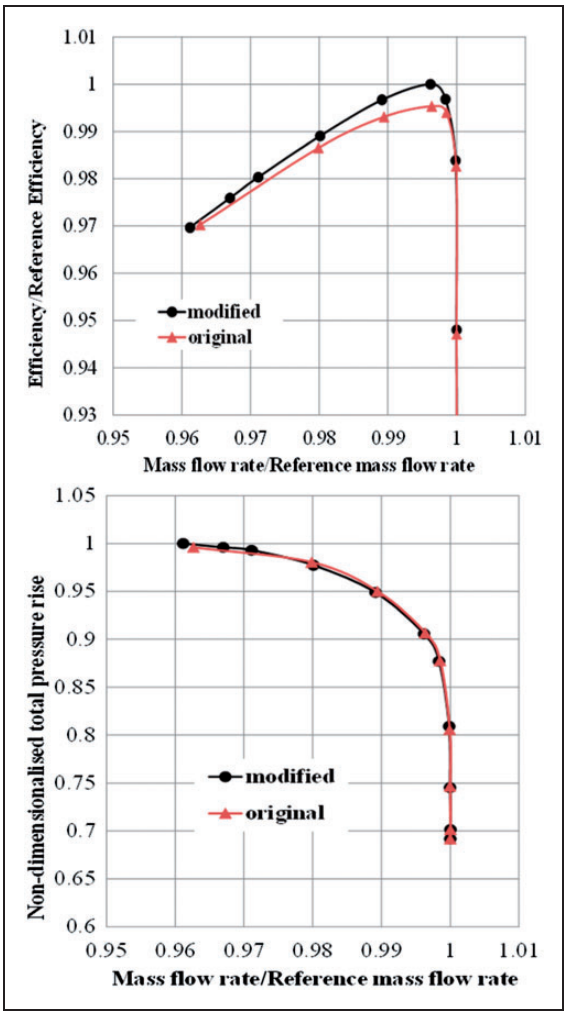

Figure 19. Comparison of the original and modified total compressor performance characteristics.

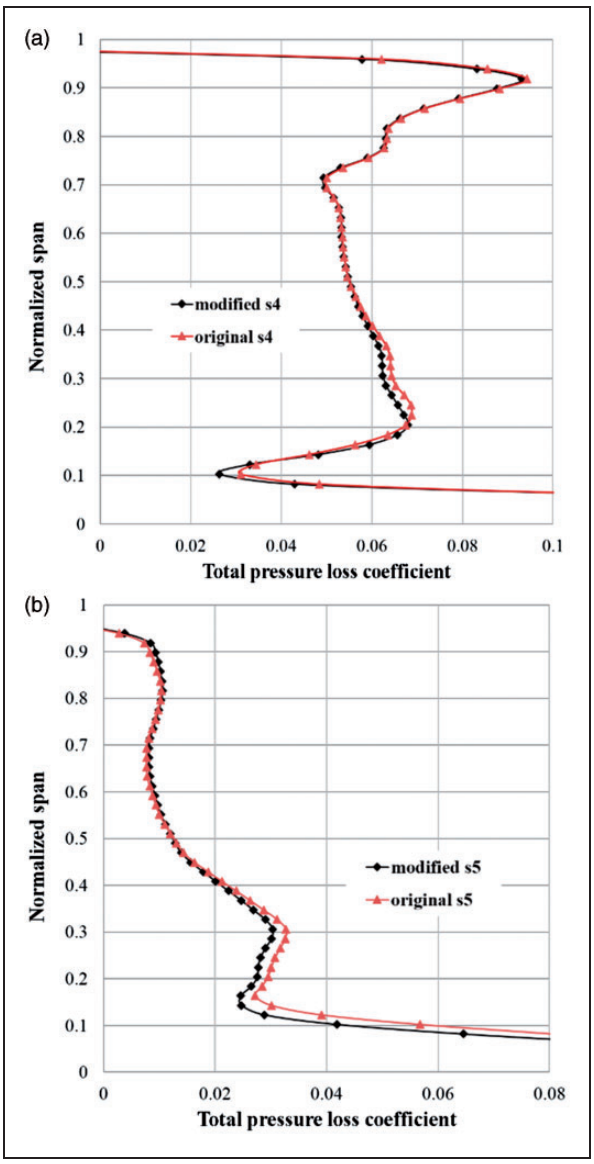

Figure 20. Comparison of original and modified total pressure losses on: (a) S4 and (b) S5.

Conclusions

The flow near the end wall region is very complicated and development pattern of the hub end wall BL thickness in a typical well-designed 5-stage compressor is summarized in its whole operating conditions. Furthermore, the effect of end wall BL on matching is discussed in details. Finally, the corresponding flow control method is used to improve the stage matching. The following conclusions can be drawn from this study:

1. The end wall BL displacement thickness increases along axial direction and the growth rate of the BL thickness dramatically increases with the operating point moving from choked condition to near surge operating point for a fixed rotating speed. The maximum end wall BL thickness influences

largely from end wall till the 4% of the average blade span near chock operating points while it influences till 12% span near peak efficiency points, moreover, till almost 16% span, near surge operating point. The average BL thickness growth rate near surge point is about 4 times than near choked operating point.
2. Moreover, the thickness of end wall BL shows insensitive to the change of rotating speed. The BL thickness of a compressor rig mainly depends on the stage pressure rise coefficient $\Delta p/\rho V_x^2$. Furthermore, the displacement thickness of BL increases through stator hub clearance and decreases across the rotor non-clearance region due to the effect of blade force deficit. The scope of end wall losses is broadened in the spanwise direction, and the pitchwise end wall BL generally tends to be skewed.
3. End wall BL produces losses, degrades the pressure rise capacity and results in the mismatching of stages. The effect of BL on pressure rise and losses gradually enlarges along the mainstream direction. The upstream stage corrected mass flow rate is further throttled and finally causes the stability limit. As for the deviation angle, up to 40% span, it is overturned close to the end wall and under-turned further away.
4. Improvement could be made to engine compressor performance by applying re-cambered designs in the end wall region. The total compressor efficiency is enhanced by 0.39 points without compromising the pressure-rise capability and the surge margin. In addition, the unsteady effect on the pattern of BL should be taken into account in the next procedure. Furthermore, the technique of re-camber will be applied to rotors in the future.

Declaration of Conflicting Interests

The author(s) declared no potential conflicts of interest with respect to the research, authorship, and/or publication of this article.

Funding

The author(s) received no financial support for the research, authorship, and/or publication of this article.

References

1. Wisler DC. Losses reduction in axial-flow compressors through low-speed model testing. *J Eng Gas Turbines Power* 1985; 107: 354–363.
2. Mellor GL and Wood GM. An axial compressor end-wall boundary layer theory. *J Fluids Eng* 1971; 93: 300–314.
3. Hirsch C. End-wall boundary layers in axial compressors. *J Eng Gas Turbines Power* 1974; 96: 413–426.
4. De Ruyck J and Hirsch C. Investigations of an axial compressor end-wall boundary layer prediction method. *J Eng Gas Turbines Power* 1981; 103: 20–33.
5. Smith LH. Casing boundary layers in multistage axial-flow compressors. *Flow research on blading*. Amsterdam: Elsevier, 1970, pp.635–647.
6. Hunter IH and Cumpsty NA. Casing wall boundary-layer development through an isolated compressor rotor. *J Eng Gas Turbines Power* 1982; 104: 805–817.
7. Lakshminarayana B and Murthy KNS. Laser-Doppler velocimeter measurement of annulus wall boundary layer development in a compressor rotor. *J Turbomach* 1988; 110: 377–385.
8. Lakshminarayana B, Pouagare M and Davino R. Three dimensional flow field in the tip region of a compressor rotor passage—Part I: Mean velocity profiles and annulus wall boundary layer. *J Eng Gas Turbines Power* 1982; 104: 760–771.
9. Stone A. *Effects of stage characteristics and matching on axial-flow-compressor performance*. New York: ASME, 1957.
10. Domercq O and Escuret JF. Tip clearance effect on high-pressure compressor stage matching. *Proc IMechE, Part A: J Power and Energy* 2007; 221: 759–767.
11. Kau HP. Compressor matching and designing for tip clearance. *Rto Lecture Series* 1998; 4-4.
12. Cumpsty NA. *Compressor aerodynamics*. 1st ed. London: Longman Scientific & Technical, 1989, pp.168–171.
13. Roberts WB, Serovy GK and Sandercock DM. Modeling the 3-d flow effects on deviation angle for axial compressor middle stages. *J Eng Gas Turbines Power* 1986; 108: 131–137.
14. Sahin FC. *Benefits of flow control on compressor blade aerodynamics*. PhD Thesis, University College London, UK, 2014.
15. Gbadebo SA, Cumpsty NA and Hynes TP. Control of three-dimensional separations in axial compressors by tailored boundary layer suction. *J Turbomach* 2008; 130: 011004.
16. Gümmer V, Goller M and Swoboda M. Numerical investigation of end wall boundary layer removal on highly loaded axial compressor blade rows. *J Turbomach* 2008; 130: 011015.
17. Jang CM, Li P and Kim KY. Optimization of blade sweep in a transonic axial compressor rotor. *JSME Int J Ser B* 2005; 48: 793–801.
18. Benin E and Biollo R. Effect of forward and aft lean on the performance of a transonic compressor rotor. *Int J Turbo Jet-Engines* 2008; 25: 13–26.
19. Beheshti BH, Teixeira JA, Ivey PC, et al. Parametric study of tip clearance—casing treatment on performance and stability of a transonic axial compressor. *J Turbomach* 2004; 126: 527–535.
20. Hergt A, Meyer R and Engel K. Experimental investigation of flow control in compressor cascades. In: *ASME turbo expo 2006: Power for land, sea, and air*. 2006: 231240. New York: ASME.
21. Vad J. Aerodynamic effects of blade sweep and skew in low-speed axial flow rotors at the design flow rate: An overview. *Proc IMechE, Part A: J Power and Energy* 2008; 222: 69–85.
22. Freeman C. Effect of tip clearance flow on compressor stability and engine performance. Von Karman Institute for Fluid Dynamics Lecture Series, 1985: 5.
23. Gallimore SJ, Bolger JJ, Cumpsty NA, et al. The use of sweep and dihedral in multistage axial flow compressor

blading—Part I: University research and methods development. *J Turbomach* 2002; 124: 521–532.
24. Gallimore SJ, Bolger JJ, Cumpsty NA, et al. The use of sweep and dihedral in multistage axial flow compressor blading—Part II: University research and methods development. *J Turbomach* 2002; 124: 521–532.
25. George KK, Sunkara SNA, George JT, et al. Investigations on stator hub end losses and its control in an axial flow compressor. In: *ASME turbo expo 2014: Turbine technical conference and exposition*. 2014: V02AT37A047-V02AT37A047. New York: ASME.
26. Luo J, Hu J, Wang Z, et al. Experimental study of effects of bowed blade on the flow field in a cantilevered stator passage. In: *ASME Turbo Expo 2014: Turbine technical conference and exposition*. 2014: V02AT37A018-V02AT37A018. New York: ASME.

Appendix

Notation

f	wall shear stress
F	blade force at boundary layer edge
H	ratio of momentum thickness and displacement thickness
L	distance between stream locations
p	static pressure
P	total pressure
PP	peak pressure ratio
s	pitchwise passage width
v	flow velocity inside boundary layer edge
V	flow velocity at boundary layer edge
y^+	first grid distance from the wall
δ	boundary layer thickness
δ^*	boundary layer displacement thickness
η_{Isen}	isentropic efficiency
η_{Pol}	polytropic efficiency
η_T	total pressure losses coefficient
π	pressure ratio
ρ	zir density
τ	clearance size
θ	boundary layer momentum thickness

Subscript

in	inlet
out	outlet
S	static
T	total
x	axial direction
Z	radial direction

Superscript

$*$	corrected parameter